Fibers and Polymers 2019, Vol.20, No.6, 1226-1235
DOI 10.1007/s12221-019-8355-8

ISSN 1229-9197 (print version)
ISSN 1875-0052 (electronic version)

Kinetic and Equilibrium Modeling of Anionic Dye Adsorption on Polyaniline Emeraldine Salt: Batch and Fixed Bed Column Studies

Sibani Majumdar, Anamika Baishya, and Debajyoti Mahanta*

Chemistry Department, Gauhati University, Assam 781014, India

(Received April 30, 2018; Revised August 27, 2018; Accepted February 6, 2019)

Abstract: In this work, removal of anionic dye Eosin Yellow (EY) by polyaniline emeraldine salt (PANI-ES) from the aqueous medium was studied by using both batch and fixed-bed column mode. Before and after the dye adsorption, the adsorbents were characterized by UV-Vis, FTIR, and XRD analysis. The morphology of the adsorbent was also studied by scanning electron microscopy (SEM). The batch adsorption study was performed by varying the initial concentration of the dye and pH. The experimental results obtained were fitted to the three isotherm models namely Langmuir, Freundlich, and Temkin and the Langmuir isotherm was found to be the best fitting model with the adsorption capacity 335 mg/g. The adsorption process followed pseudo second order kinetics. The thermodynamic study was also performed and thermodynamic parameters ΔH^{o}, ΔS^{o}, and ΔG^{o} were calculated. The adsorption experiments were also carried out in packed columns by varying some important factors like flow rate, bed height, pH, and the initial dye concentration. The experimental results obtained were fitted using Bohart-Adams, Yoon-Nelson, and Thomas models. Among the models studied, the highest adsorption capacity, 79.0 mg/g was calculated from Thomas model at pH 4 with 375 mg/*l* initial concentration, flow rate 0.3 m*l*/min, and bed height 1.4 cm.

Keywords: Polyaniline emeraldine salt, Adsorption, Thermodynamic study, Batch study, Fixed-bed column study

Introduction

The technological development and industrial revolution have introduced various industrial effluents into the ecosystem causing severe environment imbalance. The waste matter released by various industries for instance textile, leather, paper, plastics, and cosmetics are known to be harmful to ecosystem [1,2]. Dyes are the common constituent of the effluent discharged by many industries and worldwide approximately 7×10^5 tons of dye has been prepared annually and about 5 % of which is discharged directly into the water. These affect the photosynthesis process and imbalances the aquatic life by increasing the COD and BOD levels [3-5]. Again these also cause severe health damage when it comes in contact with human beings [6,7]. Eosin Yellow (EY) is one of the major dyes used in dyeing, printing ink, fluorescent pigments and also in gram staining technique [8,9]. EY may cause serious irritation in skin and eyes when comes in direct contact and also affects the kidney, liver, etc. [10,11]. Therefore, it is very vital to remove EY from wastewater. Several methods for effluents removal have been practised such as adsorption, chemical flocculation/coagulation, photodegradation, chemical oxidation, electrochemical oxidation, microbial degradation, etc., among which adsorption process is found to be the most striking and valuable because of its ease to handle, simple design, and low cost properties over the other techniques [12-15]. Moreover, the effluents treated by adsorption are free of any harmful aromatic amines and free radicals produced by other techniques such as microbial and photodegradation [16].

Several useful properties such as low production charge, high environmental stability, and the simple doping/ dedoping nature of polyaniline by acid/base treatment make it one of the most promising and extensively considered conducting polymers [17-19]. It can be synthesized easily from aniline by simple chemical or electrochemical methods [11]. It has been observed that most of the applications of PANI and hybrid materials derived from PANI are due to their conducting or semiconducting nature [20], but there are several reports where PANI and PANI based hybrid materials have been used as adsorbents for waste water treatment [21-25]. Patra and his group have developed potus alum doped polyaniline for adsorption of different anionic dyes [26], Ansari and coworkers have synthesized a composite of *p*-toluene sulfonic acid doped polyaniline with carbon nanotube and graphene oxide and the batch adsorption studies were performed for Cr(VI) and congo red dye [27]. Adsorption studies on cationic dyes like methylene blue were also done by polyaniline and polypyrrole synthesized by using carbon dot initiated polymerization process [28].

Here, we have studied the adsorption of EY by PANI-ES in both batch and fixed bed column modes. In literature it is observed that the adsorption study on PANI and PANI based hybrid materials are limited to batch mode studies only. To our knowledge, no work has been reported on the continuous flow on PANI column. The batch studies are useful for providing different adsorption parameters for pollutant removal, but the result acquired from batch adsorption studies may not be worthwhile for many wastewater systems [22,23]. As industries are not likely to use the batch adsorption technique, the study of column adsorption is

*Corresponding author: debam@gauhati.ac.in

required to know about the practical utilities of the adsorbents [4]. In the batch adsorption process, effect of the different initial concentrations of the dye and pH were investigated. It was seen that the extent of adsorption increases with increase in the initial concentration of EY, but decreases with increase in pH. The three isotherm models namely Langmuir, Freundlich, and Temkin isotherm models were fitted to the batch adsorption results. It was found that the batch adsorption results were fitted best to Langmuir isotherm model. Again the adsorption process was found to follow 2nd order kinetics. Moreover, the effects of different factors such as flow rate, initial dye concentration, bed height, and pH of the dye solution on the breakthrough curve were also studied. We have determined the uptake capacity and percentage of dye removal by varying the adsorption parameters. Thomas, Yoon-Nelson, and Bohart-Adams models were used to fit the experimental data for analyzing the column performance in removing EY from polluted water. Thus, results obtained from both studies are necessary for complete understanding of adsorption behavior by any adsorbent.

Experimental

Materials

Aniline was bought from Merck, India and distilled before use. All the other chemicals such as ammonium persulfate (APS), ammonium hydroxide, hydrochloric acid, acetone, and EY were also purchased from Merck, India. Double distilled water was used in all performed experiments.

Synthesis of Adsorbent Material

Oxidative polymerization method was used for synthesis of polyaniline emeraldine salt (PANI-ES) as described in elsewhere [21]. The detail of the synthesis procedure is given in supporting information (SI-1, Figure S1).

Characterization Techniques

The synthesized material was analyzed by using a UV-1800 Shimadzu UV/visible absorption spectrometer. The FTIR analysis was done by making pellets with dry KBr using an IR Affinity-1 Shimadzu spectrophotometer. The powder X-ray diffraction study was carried out with a Rigaku Ultima IV powder diffractometer using Cu-Kα X-radiation (λ=1.54 Å). To study the morphology of the material, scanning electron microscopy was done with a Zeiss Ultra 55 scanning electron microscope. Zeta potential analysis was carried out using a Zetasizer Nano series Nano-ZS90.

Batch Study

For the adsorption experiments in batch mode, 50 mg of PANI-ES and 50 m*l* dye solutions having different initial concentrations (100 to 500 mg/*l*) were used. All the adsorption experiments were continued for 2 h as equilibrium is reached within 2 h. 500 μ*l* of the solutions were collected at different intervals of time (0, 2, 5, 10, 20, 30, 60, and 120 min respectively) and the adsorbent particles were removed by using centrifuge. The concentrations of the dye samples were analyzed by a UV-visible absorption spectrometer (UV-1800 Shimadzu Spectrophotometer). The equilibrium uptake (q_e) was evaluated using equation (1) [29].

$$q_e = \frac{(C_0 - C_e)V}{W} \tag{1}$$

where V is the volume of the solution (l) and W is the mass of the adsorbent (g); C_0 and C_e represent the initial and equilibrium concentration of the dye solution in mg/l, respectively. The consequences of pH on dye adsorption were also investigated in the pH range 4 to 9.

Column Adsorption Experiments

Glass columns having internal diameter 1.4 cm and length 30 cm were taken for the column studies. Different amounts of adsorbent materials were employed in the columns to obtain required bed heights. At definite intervals of time, effluent samples were taken from the column and the respective concentrations of the samples were determined by spectroscopic method as discussed in batch studies. The influence of different factors such as initial dye concentration, bed height, flow rate, and pH on the breakthrough curve was studied. Different operating conditions employed in this study are reported in supporting information, Table S1. The time, at which the effluent concentration (C_t) from the column acquires 1 % and 99 % of the initial dye concentration, the breakthrough time (t_b), and column exhaustion time (t_e) were determined.

Equation (2) has been used to obtain the effluent volume, V_{eff} (ml):

$$V_{eff} = Qt_{total} \tag{2}$$

where Q in ml/min indicates the volumetric flow rate and t_{total} represents the total flow time in minute [30].

The total quantity of dye adsorbed in the column, q_{total} is estimated in mg from the area under the breakthrough curve using equation (3) and the total quantity of the dye, m_{total} (mg) used in the column can be calculated from equation (4) [31].

$$q_{total} = \frac{QC_0}{1000}\int_{t=0}^{t=t}\left(1 - \frac{C_t}{C_0}\right)dt \tag{3}$$

$$m_{total} = \frac{C_0 Qt_{total}}{1000} \tag{4}$$

where C_0 and C_t are the inlet concentration and effluent concentration of the dye at time t in mg/l, respectively.

The total dye removal percent (%R) is given by equation (5) [32]:

$$\%R = \frac{q_{total}}{m_{total}} \times 100 \quad (5)$$

Equation (6) gives the adsorption capacity in mg/g [33].

$$q_e = \frac{q_{total}}{w} \quad (6)$$

where w represents the amount of the adsorbent in g.

The mass transfer zone is estimated using equation (7):

$$Z_m = Z\left(1 - \frac{t_b}{t_e}\right) \quad (7)$$

where Z_m and Z indicate the mass transfer zone and bed height both in cm, respectively and t_b and t_e are breakthrough and exhaustion time in min, respectively.

Results and Discussion

UV-Visible Spectroscopic Analysis

The UV/Vis spectra of PANI-ES before and after the adsorption of EY are shown in Figure 1. NMP was used as solvent to record the spectra and PANI-ES was converted to polyaniline emeraldine base (PANI-EB) when it was dissolved in NMP. The peaks at around 300 nm and 630 nm appear due to π to π* transition and molecular exciton transition, respectively, which are characteristic peaks of PANI-EB [25,34]. The spectrum after adsorption shows a peak at around 520 nm due to EY, along with the characteristic peaks of PANI-EB.

FTIR Study

The FTIR spectra of PANI-ES recorded before and after adsorption of EY are shown in Figure 2. The FTIR peak observed near 3400 cm^{-1} is due to the N-H stretching mode of PANI. The band corresponding to C=C stretching of quinoid and benzoid rings of PANI appear at around 1600 cm^{-1} and 1490 cm^{-1}, respectively. The peak appearing at around 1420 cm^{-1} assigns to aromatic C-N stretching mode. The peak at 1100 cm^{-1} establishes the conductivity of PANI-ES [34-36]. It is interesting to note that slight shift of FTIR peaks to the higher frequency region for the polymeric adsorbents has been observed after adsorption of EY dye. Also, the peak intensity at 1500 and 1426 cm^{-1} are found to be decreased. Such observations may be expected due to the interaction of the polymer chain with EY, which decreases the extent of charge delocalization of the polymer chain. Thus, FTIR analysis confirms the formation of PANI-ES and a possible interaction between PANI-ES and EY.

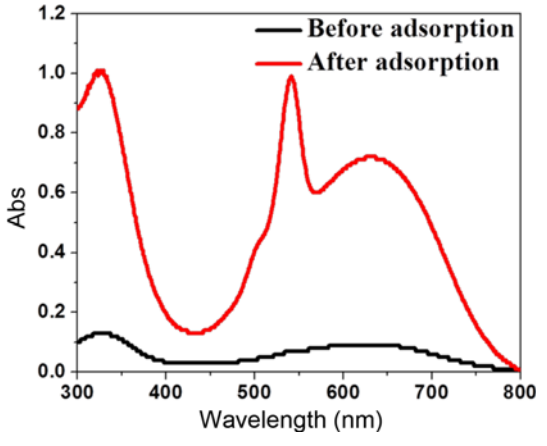

Figure 1. UV-visible spectra of PANI-ES dissolved in NMP before and after EY adsorption.

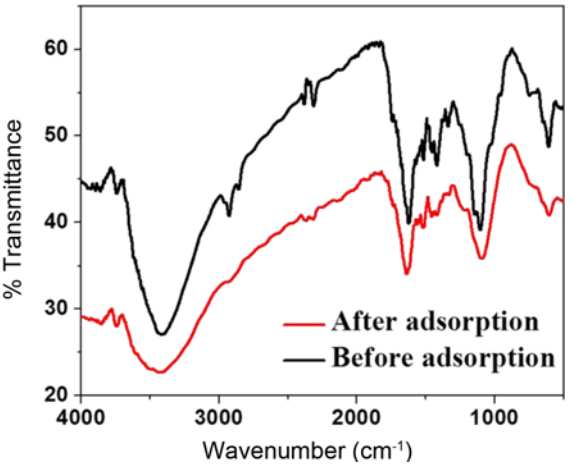

Figure 2. FTIR spectra of PANI-ES before and after EY adsorption.

Scanning Electron Micrograph Analysis

A granular form of PANI-ES is observed from the SEM micrograph as shown in Figure 3. It is also noticed from the micrograph that the material is homogeneous and the bigger particles are formed by agglomeration of the smaller one. It is apparent from Figure 3 that most of the particles are in the range of 2-10 μm.

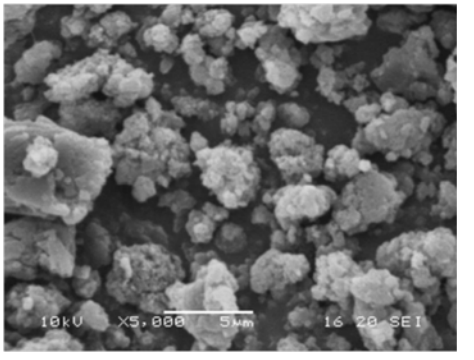

Figure 3. Scanning electron micrograph of PANI-ES.

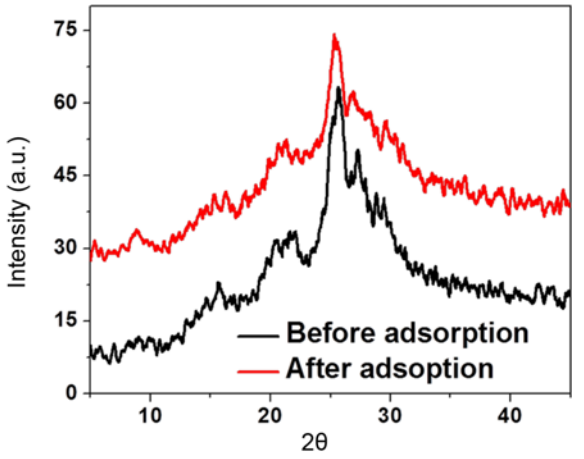

Figure 4. X-ray diffraction patterns of PANI-ES after and before adsorption of EY.

X-ray Diffraction Analysis

In the XRD pattern (Figure 4) all the characteristic features of PANI-ES are observed at 2θ=9.1, 15.7, 20.3, and 25.6 °. It also points out that there is no such considerable difference between the two plots of PANI-ES, before and after adsorption of the dye. Thus, it can be said that EY adsorption does not affect the crystallinity of PANI-ES [21]. Thus it is predicted that the adsorption takes place mainly on the surface of PANI-ES particles. There is less probability of dye molecule diffusion to the interior of swollen polymeric particles affecting the crystallinity of PANI-ES.

Zeta Potential

The zeta potential measurements were done at acidic, neutral, and basic pH to know about the effect of pH on the surface charge of the material. The zeta potential obtained for PANI-ES particles at neutral pH is (+) 0.376 mV which is increased to (+) 6.95 mV at pH 4.5. Again at pH 8, the zeta potential value obtained is (-) 21.5 mV. Thus, at neutral pH the surface charge of PANI-ES particles is positive and the positive charge density has increased at low pH, but at basic pH the surface charge becomes negatively charged. The obtained zeta potential plots are given in Figure S2.

Batch Adsorption Studies

The consequence of initial dye concentration on the adsorption behavior was studied. Figure 5(a) shows that as the dye concentration increases from 100 to 500 mg/*l*, the uptake capacity of the adsorbent increases because at higher concentration, larger number of dye molecules occupy more number of binding places of the adsorbent materials but for low dye concentration the occupation is less.

The consequence of the pH of the dye solution on adsorption was also investigated. Figure 5(b) shows that an increase in pH decreases the adsorption of EY. It is established from our previous study that partial positive

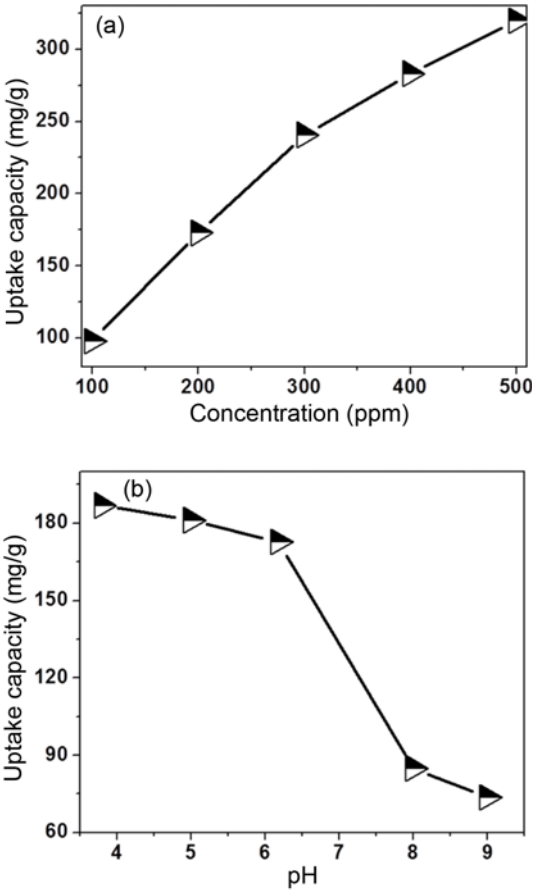

Figure 5. Adsorption capacity (a) at different initial dye concentration and (b) at different pH.

charges on the polyaniline emeraldine salt chains are responsible for anionic dye adsorption due to electrostatic interaction [23]. This explanation is also supported from the zeta potential analysis as given above. It is observed that the surface of PANI-ES is positively charged at neutral pH and on decreasing the pH the surface charged becomes more positive, whereas the surface turns into negatively charged at high pH. Therefore, at acidic pH, the PANI is in the doped form and the positive charge density on the PANI-ES particle is high, which is responsible for greater adsorption of anionic dyes at acidic pH. But at basic pH, there is a sudden decrease in the adsorption of EY due to gradual increase of negative charge density on the surface of PANI-ES particles caused by structural conversion of polyaniline emeraldine salt to polyaniline emeraldine base form. This structural change causes the repulsion between EY and negatively charged surface of PANI-EB resulting lower adsorption at higher pH.

To apply an adsorbent for practical purpose, it is necessary to analyze the experimental results with different adsorption isotherm models. The adsorption data obtained were fitted to three isotherm models accordingly Langmuir, Freundlich,

and Temkin. Langmuir model pursues the monolayer adsorption with homogeneous sharing of finite identical spots on the adsorbent surface [37]. The linear form of this model is given by equation (8):

$$\frac{C_e}{q_e} = \frac{1}{Q_0 b} + \frac{C_e}{Q_0} \tag{8}$$

The constant Q_0 and b are called Langmuir constants, where Q_0 represents the adsorption capacity in mg/g and b represents the adsorption constant in l/mg. q_e in mg/g is the adsorbate amount adsorbed per unit weight of the adsorbent and C_e in mg/l is the equilibrium adsorbate concentration. This model suggests that the extent of adsorption increases as the adsorbate concentration in the solution increased.

The Freundlich model in linear form is given by the equation (9):

$$\log q_e = \log K_F + \frac{1}{n}\log C_e \tag{9}$$

The constant K_F and n are called Freundlich constants, where K_F is related to adsorption capacity and n represents adsorption intensity [38]. Another important isotherm model is Temkin model, which can be used to calculate the heat of adsorbed molecule with the extent of coverage over the surface of the adsorbent [39]. The Temkin model in linear form is as follows:

$$q_e = B(\ln A) + B(\ln C_e) \tag{10}$$

where A (l/mg) is the equilibrium binding constant and $B=RT/b$, where b (J/mol) is related to heat of adsorption and R and T are the gas constant and absolute temperature, respectively. Figure 6 shows the fitting of experimental data in different isotherm models. It can be suggested from the R^2 values that the adsorption of EY is better fitted in the Langmuir adsorption model. The data evaluated from the adsorption isotherm models are given in Table 1.

A study of adsorption kinetics is required to have an idea on adsorption mechanism. We have fitted the obtained data in the second order kinetic model and the model in linear form is given by equation (11):

$$\frac{t}{q_t} = \frac{1}{k_s q_e^2} + \frac{1}{q_e} t \tag{11}$$

where k_s in g/mg/min represents the rate constant and q_t is the quantity adsorbed at time t in mg/g [21]. The linear plot of t/q_t versus time is shown in Figure S3 and Table S2 in the supporting information contains the results obtained from the plot. From the R^2 values, it can be suggested that the adsorption process follows the second order kinetics model and the adsorption capacities (q_e) calculated from the model

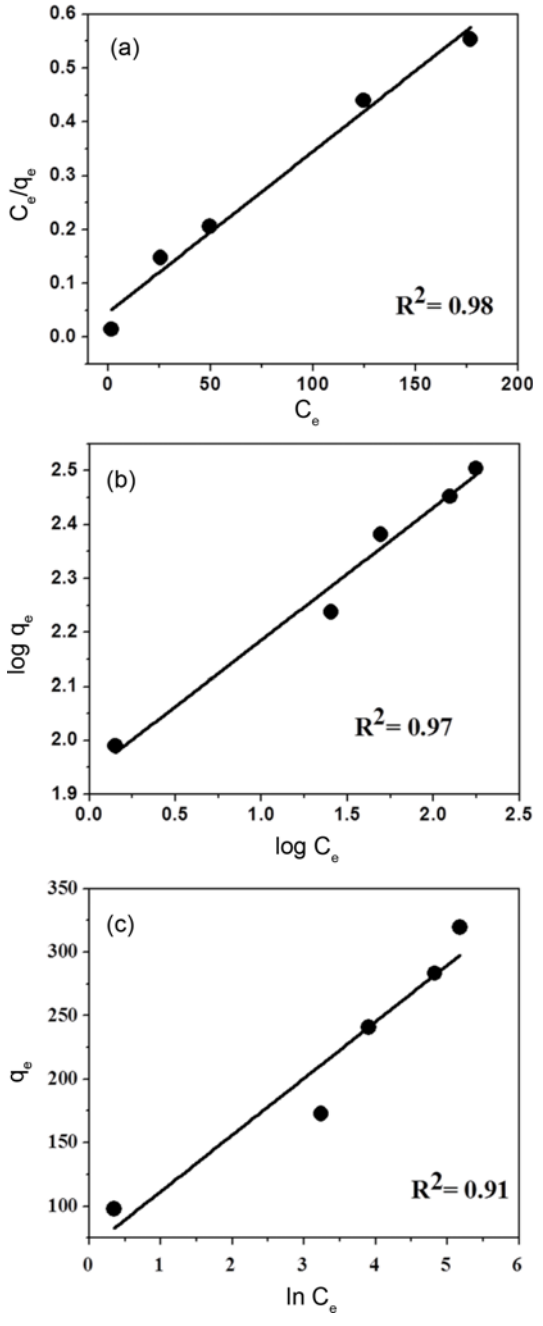

Figure 6. Plots of (a) Langmuir, (b) Freundlich, and (c) Temkin isotherm model for EY adsorption.

Table 1. Adsorption isotherm parameters

Langmuir Isotherm			Freundlich Isotherm			Temkin Isotherm		
Q_0 (mg/g)	B (l/mg)	R^2	K_F (mg/g)	n	R^2	B	A (l/mg)	R^2
335	0.064	0.98	87	4.08	0.97	44.58	2.71	0.91

are also found to be close to that of the experimental q_e values.

Thermodynamic Study

For neutral molecules or weak charged molecules such as dye molecules, thermodynamic equilibrium constant, and Langmuir equilibrium constant are numerically equal [40-42]. Thus the thermodynamic free energy change is expressed by the following equation (12):

$$\Delta G^{o} = -RT\ln K \tag{12}$$

where K is the thermodynamic equilibrium constant, R and T are the gas constant and absolute temperature, respectively.

Equilibrium constant K can be calculated from Langmuir isotherm constant by using equation (13):

$$K = 1000 b M_A \tag{13}$$

where b corresponds to the Langmuir isotherm constant in l/mg and M_A represents the molecular weight of the adsorbate EY [43].

The standard enthalpy change (ΔH^{o}) and standard entropy change (ΔS^{o}) are derived from equation (14). The slope and intercept of the plot ln$K$ versus $1/T$ gives the value of ΔH^{o} and ΔS^{o}, respectively (Figure S4).

$$\ln K = \frac{\Delta S^{o}}{R} - \frac{\Delta H^{o}}{RT} \tag{14}$$

Table S3 contains all the thermodynamic data obtained. The ΔH^{o} value obtained is 28.86 kJ/mol, the positive value indicates that the adsorption process is endothermic and its magnitude specifies that physical adsorption is mainly involved in the process. The positive value of ΔS^{o} indicates an increased randomness at the solid/solution interface during the process of adsorption. The negative ΔG^{o} value suggested the spontaneity of the adsorption process, while increase in ΔG^{o} value with increasing temperature indicates that the adsorption process is favorable at high temperature.

Column Adsorption Studies

Effect of Initial Concentration

The consequence of initial concentration on removal of EY by PANI-ES in fixed bed column has been investigated. The bed height and flow rate were kept fixed at 2 cm and 0.3 m*l*/min, respectively. An increase in the breakthrough

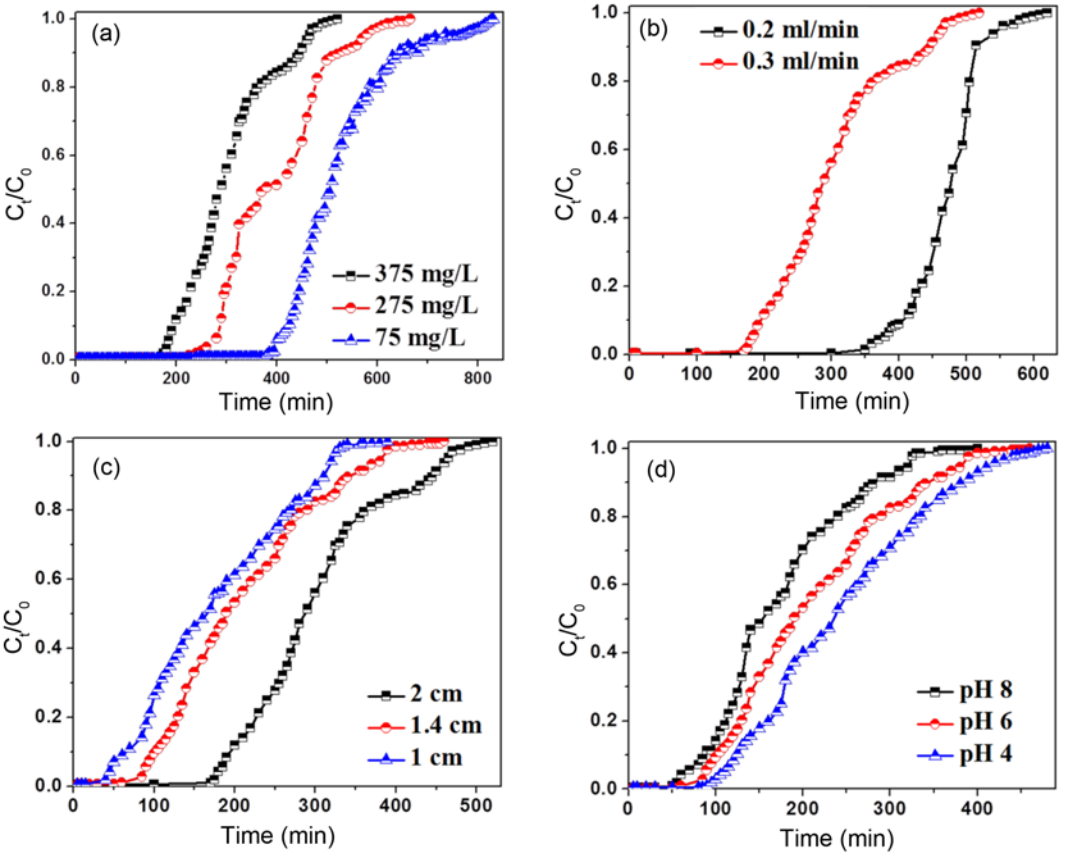

Figure 7. Breakthrough plots for (a) different initial concentration of dye, (b) different flow rate, (c) different bed height, and (d) different pH.

and exhaustion time is observed with decrease in the inlet concentration. This is because the saturation rate of the binding sites becomes slower and as a consequence the uptake capacity decreases with decrease in initial dye concentration. It is observed from Figure 7(a) that at initial concentration of 75 mg/*l*, the exhaustion time was found to be 825 min and it was decreased to 630 and 500 min for 275 and 375 mg/*l*, respectively. The uptake capacity was also enhanced with increase in initial concentration.

Effect of Flow Rate

To investigate the consequence of flow rate on the breakthrough curve adsorption experiments were carried out by varying the flow rates from 0.2 to 0.3 m*l*/min, initial concentration and bed length were kept fixed at 375 mg/*l* and 2 cm, respectively. Both the exhaustion and breakthrough time were decreased with increase in flow rate as shown in Figure 7(b). The uptake capacity also decreases at higher flow rate. The insufficient contact time of PANI-ES with EY is the reason for this behavior. The uptake capacity decreases from 70.4 to 67.5 mg/g as the flow rate increases from 0.2 to 0.3 m*l*/min.

Effect of Bed Height

To study the consequence of bed height on the breakthrough curve, adsorption experiments were done with different bed heights of 1, 1.4, and 2 cm. The bed height of 2, 1.4, and 1 cm in the column were obtained by using 0.5, 0.35, and 0.25 g of adsorbent, respectively and it is given in Figure 7(c). The initial concentration and flow rate were kept fixed at 375 mg/*l* and 0.3 m*l*/min, respectively. The exhaustion time was found to be 360, 420, and 500 min for the bed height 1, 1.4, and 2 cm, respectively. Increase in the mass transfer zone is noticed with the increase in bed length and an increase in the percentage removal of dye was also observed. As the number of binding sites increases with increase in the bed height, the adsorption capacity also increased.

Effect of pH

Same pH effect on adsorption was observed in column experiments as we noticed earlier in batch experiments. For these fixed-bed column experiments, the initial concentration, bed length, and flow rate were kept fixed at 375 mg/*l*, 1.4 cm, and 0.3 m*l*/min, respectively. The exhaustion time was found to be decreased with increase in solution pH as shown in Figure 7(d). Naturally, as the pH increased, the percentage of dye removal was also found to be decreased. The exhaustion times were recorded 465, 420, and 355 min with percentage removal of dye 50, 45, and 43 % for the pH 4, 6, and 8, respectively. All the parameters evaluated from the breakthrough curves are given in Table S4.

Modeling of the Breakthrough Curves

Bohart-Adams Model

This model follows the surface reaction theory which measures bed capacity at different breakthrough points. This model predicts that the rate of adsorption is proportional to fraction of the adsorption capacity of the adsorbent. Generally, the initial part of the breakthrough curve is explained by Bohart-Adams model (Figure S5). The linear form of Bohart-Adams equation bears a relationship between bed height (Z) and time (t) [44]. This is also known as Bed-depth service time model given by equation (15):

$$t = \frac{N_0 Z}{C_0 U} - \frac{1}{C_0 K_{AB}} \ln\left(\frac{C_0}{C_t} - 1\right) \tag{15}$$

where t indicates service time in min, N_0 in mg/*l* is the adsorption capacity, Z is the bed height in cm and U is the linear velocity in cm/min. C_0 and C_t are the initial concentration and the concentration at time t in mg/*l*, respectively. K_{AB} is the adsorption rate constant in *l*/mg/min. The value of K_{AB} and N_0 are calculated from the intercept and slope of the equation (15). At 50 % breakthrough, the last term in the equation (15) becomes zero [45] and the equation is reduced to equation (16):

$$t = \frac{N_0 Z}{C_0 U} \tag{16}$$

A plot at 35 % and 50 % breakthrough is shown in the Figure S5. Generally, the plot should be straight line that passes through the origin, but here the case is not like that, which suggests that the adsorption process takes place through some complex mechanism that involves several rate limiting steps. Thus, the simple Bohart-Adams model is not able to explain the complex adsorption mechanism. The values of N_0, evaluated from the slope of the plot were 16.6 and 13.6 mg/*l* for 35 % and 50 % breakthrough, respectively. The rate constant obtained for 35 % breakthrough was 5×10^{-5} *l*/mg/min.

Thomas Model

Thomas model is another important model that explains the adsorption behavior in a fixed-bed column. Generally Thomas model is applied on that types of adsorption processes only where external and internal diffusion limitations are absent. It was derived from the second-order kinetics and according to this model, adsorption is not controlled by the chemical reaction rather than by the mass transfer at the interface. The Thomas model in linear form is given by equation (17):

$$\ln\left[\frac{C_0}{C_t} - 1\right] = \frac{K_{Th} q_e w}{Q} - K_{Th} C_0 t \tag{17}$$

where K_{Th} in m*l*/mg/min is the Thomas constant, q_e in mg/g is the adsorption capacity, C_0 and C_t are the inlet concentration and effluent concentration of adsorbate at time t in mg/*l*, respectively, Q and W are the flow rate and mass of adsorbent in m*l*/min and g, respectively. The slope and intercept of the plot of $\ln[(C_0/C_t)-1]$ versus time gives the values K_{Th} and q_e, respectively [46].

The Thomas plots for different adsorption parameters are

shown in Figure S6. The values of correlation coefficients show the fitting of the model with the experimental data. When the inlet dye concentration increases from 75 to 375 mg/*l*, the K_{Th} was found to be decreased from 0.2 to 0.05 m*l*/mg/min while the q_e was found to increase. The greater driving force possessed by the increased inlet dye concentration may be the reason for increase in q_e. The rate constant for Thomas model decreased with increase in flow rate and decrease in pH, respectively. The calculated K_{Th} values were 0.09 and 0.05 m*l*/mg/min for flow rates 0.2 and 0.3 m*l*/min and 0.04, 0.05, and 0.06 m*l*/mg/min for pH 4, 6, and 8 respectively. While for different bed heights the Thomas constant was found to be almost constant at 0.05 m*l*/mg/min. The uptake capacity decreases with increase in pH as expected. Standard error estimate method was used to compare the calculated K_{Th} values with the experimental values [45]. The method is expressed by equation (18):

$$SE = \sqrt{\left[\Sigma \frac{\{q_{e(\text{exp.})} - q_{e(\text{calc.})}\}^2}{N}\right]} \quad (18)$$

where $q_{e(\text{exp.})}$ and $q_{e(\text{calc.})}$ represents the experimental adsorption capacity and the adsorption capacity values calculated from the model, respectively.

Yoon-Nelson Model

Yoon-Nelson model is relatively a simple model and independent of the type of the adsorbent. This model is given by the following linear equation (19):

$$\ln\left(\frac{C_t}{C_0 - C_t}\right) = K_{YN}t - K_{YN}\tau \quad (19)$$

where K_{YN} in min^{-1} indicates the Yoon and Nelson's constant and τ in min represents the time required for keeping half of the initial adsorbate [38]. The Yoon-Nelson plots are given in Figure S7. It was observed that, K_{YN} increased with increase in inlet ion concentration, but τ was found to be decreased. While with increase in flow rate both K_{YN} and τ were decreased. The Yoon-Nelson rate constant K_{YN} was found constant at 0.02 min^{-1} for all bed heights. It was also found constant at 0.02 min^{-1} at all pH. All the parameters evaluated from Thomas and Yoon-Nelson plots are given in Table 2.

Mechanism

The adsorption mechanism of EY on the PANI-ES surface is shown in the Scheme 1. PANI-ES particles have positive surface charge and EY is dissociated into ionic form (Scheme 1(A)). The dissociation constant of the dye increases with the decrease in pH. In the same time with decrease in pH, the surface charge on PANI particles become more and more positive. This leads to the increase in electrostatic interaction between PANI-ES particles and dye anions at lower pH causing greater removal of dyes. The adsorption of the dye is also confirmed from the UV-visible spectra shown in Figure 1, where the characteristic peak of the dye is observed in the spectra after adsorption. The FTIR studies also indicate an interaction between PANI-ES chain

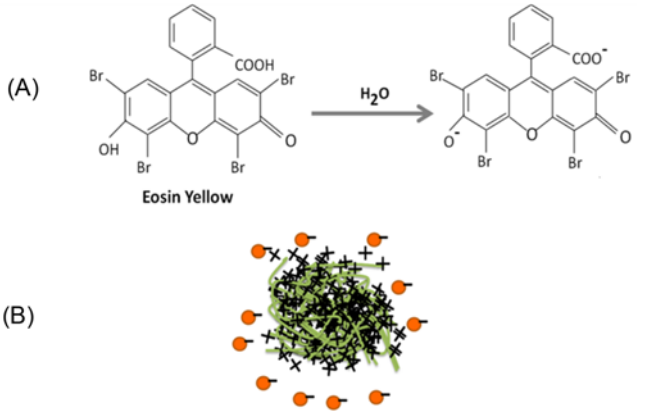

Scheme 1. Schematic diagram for adsorption of EY on PANI-ES surface; (A) ionization of EY and (B) electrostatic interaction between EY dye anion and PANI-ES Surface.

Table 2. Results obtained from the Thomas and Yoon-Nelson model

C_0 (mg/*l*)	Z (cm)	Flow rate (m*l*/min)	pH	K_{YN} (min^{-1})	τ (calc.) (min)	K_{Th} (m*l*/mg/min)	q_e (calc.) (mg/g)	q_e (exp.) (mg/g)	SE	R^2
375	2	0.3	6	0.020	304	0.05	65.9	67.5	0.23	0.95
275	2	0.3	6	0.018	400	0.06	65.5	60.7	0.67	0.97
75	2	0.3	6	0.015	531	0.20	24.0	23.7	0.02	0.94
375	1	0.3	6	0.02	199	0.05	77.9	65.4	1.75	0.93
375	1.4	0.3	6	0.02	214	0.05	68.8	67.0	0.23	0.96
375	2	0.3	6	0.02	304	0.05	65.9	67.5	0.23	0.95
375	2	0.2	6	0.03	468	0.09	70.2	70.4	0.03	0.98
375	2	0.3	6	0.02	304	0.05	65.9	67.5	0.23	0.95
375	1.4	0.3	4	0.02	242	0.04	79.0	78.4	0.07	0.95
375	1.4	0.3	6	0.02	214	0.05	68.8	67.0	0.23	0.95
375	1.4	0.3	8	0.02	180	0.06	56.2	55.1	0.15	0.96

and the dye particles, whereas the XRD analysis indicates the involvement of only the surface of PANI-ES in the adsorption process. The zeta potential values of PANI-ES particles at different pHs also support the proposed mechanism. When the dye adsorbed PANI-ES particles were treated with 1 M NH_4OH solution, the PANI-ES particles were converted into PANI-EB form with negative surface charge that results electrostatic repulsion and finally desorption of the dye molecules.

Conclusion

From this study, we can conclude that PANI-ES acts as an excellent adsorbent for anionic dye EY. Detailed adsorption studies in both batch and continuous fixed bed column modes were executed at different experimental conditions. The adsorption process followed pseudo second order kinetic model with Langmuir adsorption capacity 335 mg/g. In column studies, the behavior of the breakthrough curves were analyzed by varying the factors like initial dye concentration, bed height, flow rate, and pH. The breakthrough time was found to be decreased with decrease in bed height and increase in flow rate and initial dye concentration. From the column studies, the highest adsorption capacity obtained was 78.4 mg/g for initial concentration 375 mg/*l* with the reaction condition of pH 4, 0.3 m*l*/min flow rate, and 1.4 cm bed height. The adsorption capacity obtained from Thomas model was 79.0 mg/g at the same reaction conditions. From this work it has been found that PANI-ES has a good adsorption capacity for the anionic dye EY. From the dynamic study it is observed that PANI-ES have a good potential for large scale waste water treatment.

Acknowledgement

The authors thank Assam Science Technology and Environment Council (ASTEC) for financial support [Grant No. ASTEC/S&T/192(153)/14-15/4247]. Sibani Majumdar thanks Council of Scientific and Industrial Research (CSIR), Government of India, for financial support in the form of Senior Research Fellowship.

Electronic Supplementary Material (ESM) The online version of this article (doi: 10.1007/s12221-019-8355-8) contains supplementary material, which is available to authorized users.

References

1. M. T. Uddin, M. Rukanuzzaman, M. M. R. Khan, and M. A. Islam, *J. Environ. Manage.*, **90**, 3443 (2009).
2. R. Das, M. Bhaumik, S. Giri, and A. Maity, *Ultrason. Sonochem.*, **37**, 600 (2017).
3. M. Tanzifi, S. H. Hosseini, A. D. Kiadehi, M. Olazar, K. Karimipour, R. Rezaiemehr, and I. Ali, *J. Mol. Liq.*, **244**, 189 (2017).
4. M. E. Fernandez, G. V. Nunell, P. R. Bonelli, and A. L. Cukierman, *Bioresour. Technol.*, **106**, 55 (2012).
5. F. Fu, Z. Gao, L. Gao, and D. Li, *Ind. Eng. Chem. Res.*, **50**, 9712 (2011).
6. R. Ansari and Z. Mosayebzadeh, *Iran. Polym. J.*, **19**, 51 (2010).
7. T. Maneerung, J. Liew, Y. Dai, S. Kawi, C. Chong, and C. H. Wang, *Bioresour. Technol.*, **200**, 350 (2016).
8. A. Mittal, D. Jhare, and J. Mittal, *J. Mol. Liq.*, **179**, 133 (2013).
9. E. Franciscon, M. J. Grossman, J. A. R. Paschoal, F. G. R. Reyes, and L. R. Durrant, *Springer Plu*s, **1**, 37 (2012).
10. M. M. Ayad and A. A. El-Nasr, *J. Nanostruct. Chem.*, **3**, 3 (2012).
11. P. Veerakumar, J. Tharini, M. Ramakrishnan, I. Panneer Muthuselvam, and K. C. Lin, *ChemistrySelect*, **2**, 3598 (2017).
12. S. Majumdar, J. Nath, and D. Mahanta, *J. Environ. Chem. Eng.*, **6**, 2588 (2018).
13. D. Mahanta, U. Manna, G. Madras, and S. Patil, *ACS Appl. Mater. Interfaces*, **3**, 84 (2011).
14. M. R. Torres, C. G. Bouzan, and M. Crespi, *Desalination*, **252**, 53 (2010).
15. S. P. D. Monte Blanco, F. B. Scheufele, A. N. Modenes, F. R. Espinoza-Quinones, P. Marin, A. D. Kroumov, and C. E. Borba, *Chem. Eng. J.*, **307**, 466 (2017).
16. R. Ansari, Z. Mosayebzadeh, M. B. Keivani, and A. M. Khah, *J. Adv. Sci. Res.*, **2**, 27 (2011).
17. D. Mahanta, N. Munichandraiah, G. Madras, S. Radhakrishnan, and S. Patil, *Synth. Met.*, **161**, 659 (2011).
18. P. Baruah and D. Mahanta, *Bull. Mater. Sci.*, **39**, 875 (2016).
19. C. O. Baker, X. Huang, W. Nelson, and R. B. Kaner, *Chem. Soc. Rev.*, **46**, 1510 (2017).
20. S. Bhadra, D. Khastgir, N. K. Singha, and J. H. Lee, *Prog. Polym. Sci.*, **34**, 783 (2009).
21. D. Mahanta, G. Madras, S. Radhakrishnan, and S. Patil, *J. Phys. Chem. B*, **112**, 10153 (2008).
22. D. Mahanta, G. Madras, S. Radhakrishnan, and S. Patil, *J. Phys. Chem. B*, **113**, 2297 (2009).
23. S. Majumdar, U. Saikia, and D. Mahanta, *J. Chem. Eng. Data*, **60**, 3382 (2015).
24. M. Jaymand, *Polym. Sci.*, **38**, 1287 (2013).
25. M. Tanzifi, M. Tavakkoli Yaraki, M. Karami, S. Karimi, A. Dehghani Kiadehi, K. Karimipour, and S. Wang, *J. Colloid Interface Sci.*, **519**, 154 (2018).
26. B. N. Patra and D. Majhi, *J. Phys. Chem. B*, **119**, 8154 (2015).
27. M. O. Ansari, R. Kumar, S. A. Ansari, S. P. Ansari, M. A. Barakat, A. Alshahrie, and M. H. Cho, *J. Colloid Interface Sci.*, **496**, 407 (2017).
28. M. Maruthapandi, V. B. Kumar, J. H. T. Luong, and A.

Gedanken, *ACS Omega*, **3**, 7196 (2018).
29. X. Yu, C. Wei, and H. Wu, *Sep. Purif. Technol.*, **156**, 489 (2015).
30. P. D. Saha, S. Chakraborty, and S. Chowdhury, *Colloids Surf. B*, **92**, 262 (2012).
31. K. Vijayaraghavan, J. Jegan, K. Palanivelu, and M. Velan, *Chem. Eng. J.*, **106**, 177 (2005).
32. Q. Yu, J. T. Matheickal, P. Yin, and P. Kaewsarn, *Water Res.*, **33**, 1534 (1999).
33. M. C. D. Hoces, G. B. Garcia, A. R. Galvez, and M. A. Martin-Lara, *Ind. Eng. Chem. Res.*, **49**, 12587 (2010).
34. D. Dutta, T. K. Sarma, D. Chowdhury, and A. Chattopadhyay, *J. Colloid Interface Sci.*, **283**, 153 (2005).
35. S. Tao, B. Hong, and Z. Kerong, *Spectrochim. Acta Mol. Biomol. Spectrosc.*, **66**, 1364 (2007).
36. A. Drelinkiewicz, M. Hasik, and M. Choczynski, *Mater. Res. Bull.*, **33**, 739 (1998).
37. S. Qiao, Q. Hu, F. Haghseresht, X. Hu, and G. Q. Lu, *Sep. Purif. Technol.*, **67**, 218 (2009).
38. X. Y. Huang, J. P. Bin, H. T. Bu, G. B. Jiang, and M. H. Zeng, *Carbohydr. Polym.*, **84**, 1350 (2011).